SCIENCE CHINA
Physics, Mechanics & Astronomy

Ga_{Zn}-V_{Zn} acceptor complex defect in Ga-doped ZnO

Tang AiHua, Mei ZengXia, Hou YaoNan, Liu LiShu, Venkatachalapathy Vishnukanthan, Azarov Alexander, Kuznetsov Andrej and Du XiaoLong

Citation: SCIENCE CHINA Physics, Mechanics & Astronomy **61**, 077311 (2018); doi: 10.1007/s11433-018-9195-7

View online: http://engine.scichina.com/doi/10.1007/s11433-018-9195-7

View Table of Contents:http://engine.scichina.com/publisher/scp/journal/SCPMA/61/7

Published by the Science China Press

Articles you may be interested in

Electronic structure of ZnO and its defects
Science in China Series A-Mathematics **44**, 1174 (2001);

Effect of intrinsic defects on p-type conductivityof ZnO:(In, N) thin films
SCIENTIA SINICA Physica, Mechanica & Astronomica **48**, 047303 (2018);

Implantation induced defects and electrical properties of Sb-implanted ZnO
SCIENCE CHINA Technological Sciences **58**, 1333 (2015);

ZnO nanorod arrays: Field-assisted growth in aqueous solution and field emission properties
SCIENCE CHINA Technological Sciences **55**, 3176 (2012);

ANOMALOUS V-I CHARACTER IN n-Ge SEMICONDUCTOR OF ACCEPTOR HEAT DEFECT COMPENSATION AT ROOM TEMPERATURE
Chinese Science Bulletin **36**, 1606 (1991);

SCIENCE CHINA
Physics, Mechanics & Astronomy

SCIENCE CHINA
Physics, Mechanics & Astronomy

CrossMark click for updates

•Article•

July 2018 Vol. 61 No. 7: 077311
https://doi.org/10.1007/s11433-018-9195-7

Ga_{Zn}-V_{Zn} acceptor complex defect in Ga-doped ZnO

AiHua Tang[1,3], ZengXia Mei[1*], YaoNan Hou[1], LiShu Liu[1], Vishnukanthan Venkatachalapathy[2], Alexander Azarov[2], Andrej Kuznetsov[2], and XiaoLong Du[1,3*]

[1] *Key Laboratory for Renewable Energy, Beijing National Laboratory for Condensed Matter Physics, Institute of Physics, Chinese Academy of Sciences, Beijing 100190, China;*
[2] *Department of Physics, Centre for Materials Science and Nanotechnology, University of Oslo, Oslo N-0316, Norway;*
[3] *School of Physical Sciences, University of Chinese Academy of Sciences, Beijing 100049, China*

Received February 8, 2018; accepted March 6, 2018; published online March 27, 2018

Gallium (Ga)-doped ZnO is regarded as a promising plasmonic material with a wide range of applications in plasmonics. In this study, zinc self-diffusion experiments are adopted to disclose the nature of the dominant compensating defect in Ga-doped ZnO isotopic heterostructures. The $(Ga_{Zn}$-$V_{Zn})^-$ complex defect, instead of the isolated V_{Zn}^{2-}, is identified as the predominant compensating acceptor center responsible for the low donor doping efficiency. The comparative diffusion experiments operated by the secondary ion mass spectrometry reveal a ~0.78 eV binding energy of this complex defect, which well matches the electrical activation energy derived from the temperature-dependent Hall effect measurements (~(0.82±0.02) eV). These findings contribute to an essential understanding of the $(Ga_{Zn}$-$V_{Zn})^-$ complex defect and the potential engineering routes of heavily Ga-doped ZnO.

Ga-doped ZnO, complex defect, self-diffusion

PACS number(s): 61.72.Ji, 71.55.Gs, 61.72.Cc

Citation: A. H. Tang, Z. X. Mei, Y. N. Hou, L. S. Liu, V. Venkatachalapathy, A. Azarov, A. Kuznetsov, and X. L. Du, Ga_{Zn}-V_{Zn} acceptor complex defect in Ga-doped ZnO, Sci. China-Phys. Mech. Astron. **61**, 077311 (2018), https://doi.org/10.1007/s11433-018-9195-7

1 Introduction

As a quintessential oxide semiconductor, zinc oxide remains the subject of intense study because of its excellent optical and optoelectronic properties. Heavily doped zinc oxide (ZnO) has been extensively explored and utilized as transparent conductive electrodes in various fields, such as displays, photovoltaics, and smart windows [1-3]. Inspiringly, ZnO, where heavy doping can produce a metallic dielectric function, has been identified as a promising plasmonic material with low plasmonic loss for the infrared spectral range, even up to telecommunication wavelengths [4-7]. In recent years, heavily gallium (Ga)-doped ZnO as a tunable metal has enabled the realization of tailoring surface-plasmon-polariton (SPP) dispersion relations in a wide range [8]. Furthermore, an ultrafast nonlinear response of bulk plasmons has been observed in Ga-doped ZnO layers [9]. However, achieving a higher doping efficiency is still challenging and impeded by the significant compensation phenomenon. The necessity of high conductivity in plasmonic materials raises concerns about the inevitable doping compensation effect caused by the point defects in Ga-doped ZnO.

In general, point defects hold a major influence on the physical properties of semiconductors considering that they dominate various diffusion mechanisms involved in doping and its limitation. The origin of the doping compensation effect in heavily doped ZnO is still under debate and com-

*Corresponding authors (ZengXia Mei, email: zxmei@iphy.ac.cn; XiaoLong Du, email: xldu@iphy.ac.cn)

© Science China Press and Springer-Verlag GmbH Germany 2018

Downloaded to IP: 159.226.35.185 On: 2018-04-02 15:10:52 http://engine.scichina.com/doi/10.1007/s11433-018-9195-7

monly attributed to two mechanisms: Zn vacancy (V_{Zn}), an acceptor in its isolated form, and V_{Zn}-related defect complexes formed by V_{Zn} and donor impurities (e.g., Ga_{Zn}-V_{Zn} and Al_{Zn}-V_{Zn} complexes) [10-13]. Thus, the confirmation of the compensating defect species and the revelation of its energetics are both of fundamental and practical interests in terms of the possibly delicate control and engineering of the defect population and useful properties.

The electronic structure and the thermodynamic stability of different types of point defects in ZnO, including isolated V_{Zn} and Ga_{Zn}-V_{Zn}, have been widely calculated [11,14-17], which was suggested to account for the optical and electrical measurements and some complementary properties of the point defects reported by other experimental techniques [18-20]. However, the theoretically derived defect energetics (formation energies as a function of the Fermi-level position and the chemical potential as well as the transition levels) in ZnO exhibits a huge controversy probably because of the finite-supercell formalism and the inaccurate description of the band structure [21]. The energetics of V_{Zn}-related point defects lacks reliable experimental data. The V_{Zn} energetics was previously validated from zinc self-diffusion measurements in the isotopic heterostructures of undoped and *in situ*-doped ZnO [22]. A more complicated Ga_{Zn}-V_{Zn} complex defect remains challenging to differentiate from isolated V_{Zn}, not to mention exploring its energetic properties.

In the present work, secondary ion mass spectrometry (SIMS) combined with temperature-dependent Hall-effect (TDH) measurements was employed to identify the $(Ga_{Zn}$-$V_{Zn})^{-}$ complex defect as the predominant acceptor center in Ga-doped ZnO and investigate its compensation behavior and thermodynamic characteristics. SIMS in conjunction with isotope tracing atoms is a very powerful approach for studying point defects because the diffusion phenomenon is closely associated with the defect formation process [22-26]. The comparative diffusion experiments revealed that $(Ga_{Zn}$-$V_{Zn})^{-}$, instead of the isolated V_{Zn}^{2-}, is the predominant compensating defect in the Ga-doped ZnO. The derived binding energy (~0.78 eV) agreed well with the electrical activation energy obtained from the TDH measurements.

2 Experiments

Two series of samples were in focus herein: ZnO isotopic double-layer heterostructures for the self-diffusion study denoted with the initial 'D', and ZnO single-layer films for the TDH measurement denoted with the initial 'S'. Two sorts of zinc sources were adopted in the synthesis of zinc-isotope Ga-doped ZnO heterostructure samples on *c*-oriented sapphire substrates by radio frequency plasma assisted molecular beam epitaxy (rf-MBE): one was in its natural isotopic ratio (labeled as ^{n}Zn), and the other was artificially enriched with 99.4% ^{64}Zn (labeled as ^{64}Zn). Ga-doped zinc-isotope ZnO heterostructures were synthesized with a top ^{n}ZnO:Ga layer on a bottom ^{64}ZnO:Ga layer, as schematically illustrated in the inset of Figure 1(a). Note that the ^{68}Zn isotope atoms in the top ^{n}ZnO layer were chosen as the diffusion source, while the bottom ^{64}ZnO layer was the diffusion space. Reflection high-energy electron diffraction was applied *in situ* to monitor the whole epitaxial growth process (Figure S1, Supporting information online). Diffusion anneals were performed in air for 2 h in a temperature range of 873-973 K. The concentration depth profiles of the Zn isotopes and dopants were characterized by SIMS with a Hiden MAXIM Analyzer. For the SIMS analysis, 5 keV Ar^{+} ions with 200 nA current were used as the primary beam raster over an area of 200 μm×200 μm. The signal-to-concentration calibration was performed using standard ^{n}ZnO and ^{64}ZnO samples as a reference. The conversion of SIMS sputtering time-to-depth profiles was performed by measuring the crater depth using a Dektak 8 profilometer (Germany) and assuming a constant erosion rate. The TDH measurements were performed in an HL5500PC Hall Effect Measurement System (Canada).

3 Results and discussion

The formation energy (E^{f}) of a point defect depends linearly

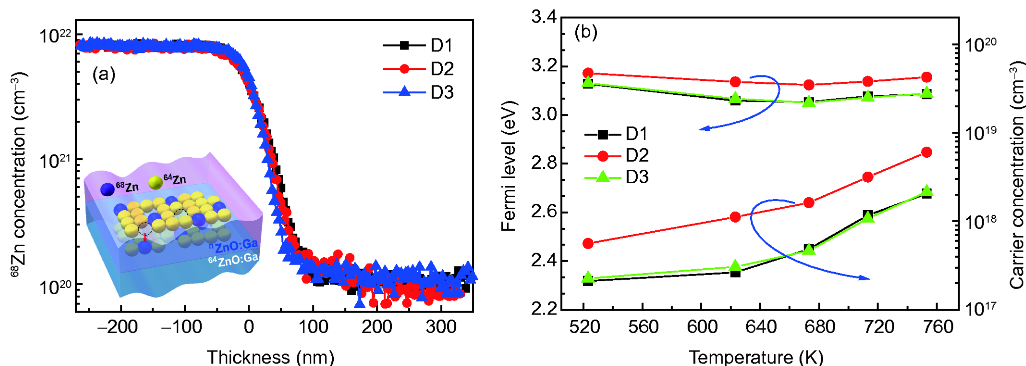

Figure 1 (Color online) (a) ^{68}Zn concentration versus depth profiles in the as-grown D1-D3. A schematic illustration of the isotopic sample structure and the ^{68}Zn diffusion source is shown in the inset; (b) Fermi level and carrier concentration versus temperature in the range of 523-753 K.

Downloaded to IP: 159.226.35.185 On: 2018-04-02 15:10:52 http://engine.scichina.com/doi/10.1007/s11433-018-9195-7

on the chemical potential (μ) and the Fermi level (E_F). The lower carrier concentration and mobility in O-rich Ga-doped ZnO [27,28] implied the existence of acceptor-like point defects with a lower E^f in O-rich conditions. One possible candidate (i.e., interstitial oxygen (O_i)) can be reasonably excluded considering its relatively high formation energy and instability [14,29]. Meanwhile, intrinsic V_{Zn} and dopant-induced extrinsic V_{Zn}-related complex defects are still under debate. In the present work, the Ga-doped ZnO isotopic heterostructures were conceived and prepared by rf-MBE with designed growth conditions, such as Zn/O-rich growth limit and Fermi level. Note that although the rf-MBE conditions were away from thermal equilibrium, they are expected to capture the changing trends of the chemical potential from O- to Zn-rich growth limits [11]. Therefore, the amount and the species of these V_{Zn}-related compensation defects can be controlled to advantage the identification of their natures and energetic properties because of their different dependence on the chemical potential and the Fermi level [14,16,22,23].

The growth conditions, including ^{64}Zn (^{n}Zn) and O fluxes, as well as the Ga dopant content, were kept the same for both the top and bottom ZnO:Ga layers in each sample, respectively. For different self-diffusion samples, the ^{64}Zn and ^{n}Zn fluxes changed, while the O flux remained constant in making the concentrations of the compensating defects in the samples vary from the Zn- to O-rich growth limit. The ^{64}Zn and ^{n}Zn fluxes were the same for D1 and D2 (Zn rich), but decreased for D3 (O rich). In contrast, D1 and D3 had a similar Ga concentration (~1×10^{19} cm^{-3} and ~2×10^{19} cm^{-3}, respectively), which was one order of magnitude lower than that of D2 (~1×10^{20} cm^{-3}). D1 was a reference sample with the least compensation defects because it was prepared under O-poor and fewer Ga dopant conditions [11,27,30]. In addition, *in situ* pre-annealing was deliberately performed at the bottom ^{64}ZnO:Ga layer before the deposition of the top ^{n}ZnO:Ga layer in D1 to dissociate the existing complex defects [11]. Table 1 shows an overview of these samples. The Zn isotopic atom's self-diffusion profiles in these samples will reflect the dependence of the Zn-related defect formation on the Zn/O-rich growth condition and Fermi level. Consequently, we can figure out its species and energetic properties.

The curves in Figure 1(a) show the ^{68}Zn concentrations versus depth profiles in the as-grown D1-D3. Interestingly, the ^{68}Zn tracing atoms in these samples manifested nearly identical profiles, suggesting that the as-grown Zn diffusion-related defects almost did not change with the varied Zn/O-rich growth limit and Fermi level, which will be discussed later. In addition, the Fermi levels E_F (T) of D1-D3 were derived by applying the TDH effect measurements in a temperature range of 523–753 K (Figure 1(b)). The E_F levels of D1 and D3 almost remained the same as expected, but lower than that of D2 at the corresponding temperatures.

As illustrated in Figure 2(a), the ^{68}Zn atom diffusion in D1 became more pronounced at the elevated annealing temperatures. This result was the same for D2 and D3 (not shown here). Taking the curves annealed at 923 K as an example, the diffusion of the ^{68}Zn atoms was much more enhanced in the order of D2, D3, and D1 (Figure 2(b)). These findings indicated that the defects mediating the diffusion process were more favorable under O-rich and high E_F conditions. Considering that only V_{Zn} and Zn_i can be the candidates dominating the self-diffusion process, the diffusing mechanism can be ascribed to the V_{Zn} defect. This finding was consistent with the broad consensus of the V_{Zn}-mediated diffusion in ZnO [22,31,32].

The diffusion profiles were simulated using second Fick's law applying reflective boundary conditions with the as-grown profile as the initial condition to obtain the Zn self-diffusion coefficient (i.e., diffusivity D) [22,23]. Based on the Arrhenius plots of the D values versus the corresponding reciprocal absolute temperatures presented in Figure 3, the diffusion activation enthalpy ΔH_a can be extracted as (1.49±0.05), (2.26±0.04), and (2.28±0.03) eV for D1, D2, and D3, respectively.

ΔH_a of the diffusion defect can be expressed as the sum of the formation enthalpy ΔH_f and the migration enthalpy ΔH_m controlled by a thermally activated intrinsic point defect mediated process. Under this assumption, for a certain point defect, ΔH_m will not be affected by E_F and μ, and ΔH_f is linearly related to E_F and μ. Specifically for V_{Zn}, ΔH_f and ΔH_a

Table 1 Growth conditions and electrical properties of the D- and S-series samples [a)]

Sample name	Substrate temperature (K)	Growth limits	Ga concentration (cm^{-3})	Thickness (nm)	Carrier concentration (cm^{-3})	Mobility (cm^2 V^{-1} s^{-1})
D1	873	Zn rich	~1×10^{19}	620	-4.96×10^{17} *	20.7 *
D2	873	Zn rich	~1×10^{20}	680	-7.37×10^{17}	24.2
D3	873	O rich	~2×10^{19}	670	-4.80×10^{17}	17.8
S1	873	Zn rich	~2×10^{20}	350	-9.88×10^{17}	17.5
S1 AN (annealed at 1023 K)	–	–	–	–	-6.81×10^{19}	55.2

a) *An *in-situ* pre-anneal treatment was performed at the bottom ^{64}ZnO:Ga layer of D1 to further decrease the compensation defects in the bottom diffusion space layer.

Downloaded to IP: 159.226.35.185 On: 2018-04-02 15:10:52 http://engine.scichina.com/doi/10.1007/s11433-018-9195-7

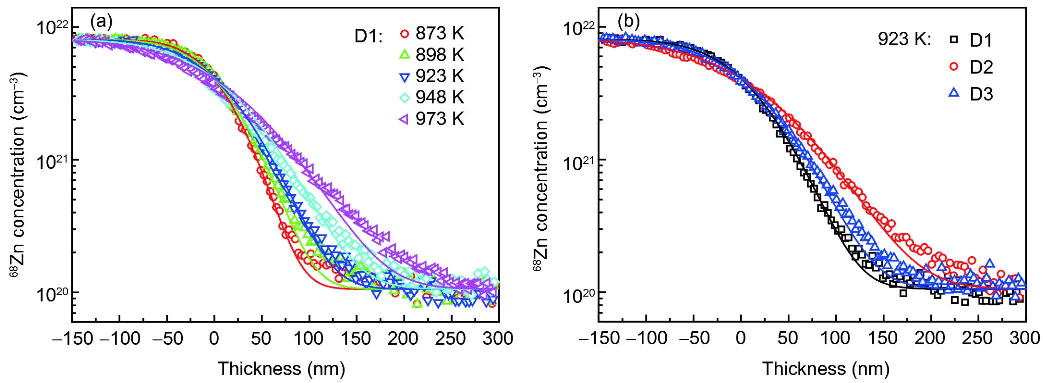

Figure 2 (Color online) Diffusion profiles of the ^{68}Zn concentrations in the annealed D1-D3. D1 after annealing between 873 and 973 K (a) and D1-D3 after annealing at 923 K (b).

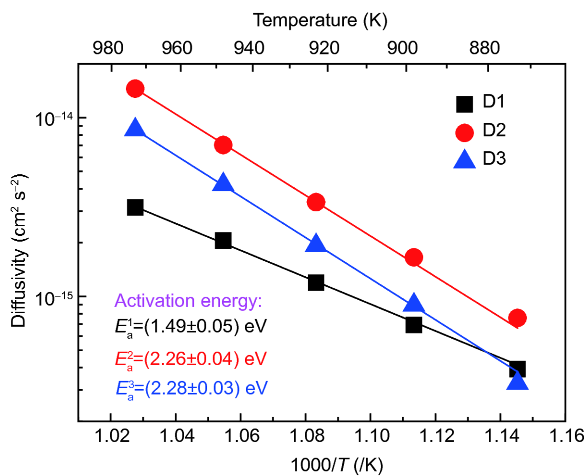

Figure 3 (Color online) Arrhenius plots of the extracted ^{68}Zn self-diffusion coefficient D versus the reciprocal temperature 1000/T. The solid lines show the best fits to the self-diffusion coefficients. The inset manifests the obtained activation energies for D1-D3.

should decrease under more O-rich and higher E_F conditions. The relatively low ΔH_a ((1.49±0.05) eV) for D1 was basically equal to the theoretically predicted migration barrier (~1.4 eV) for V_{Zn} [14,19], suggesting that a direct diffusion mechanism without the need of forming thermally activated defects (the diffusing atoms simply jumped into the neighboring vacancy sites) dominated the diffusion process as expected (i.e., the activation enthalpy of D1 was essentially determined by the migration enthalpy) [23,33]. However, ΔH_a for D2 (higher E_F) and D3 (more O-rich) was larger than D1, differing from the abovementioned condition (ΔH_a should decrease under O-rich and high E_F conditions) and from our previous results on the Zn self-diffusion via thermally activated intrinsic V_{Zn} defect at a relatively high-temperature region [22].

First, the influence of the dislocation motion and the grain boundary diffusion can be excluded because of the similar crystal qualities for all samples (Figure S2). Their diffusion coefficients were a few orders of magnitude higher than those of volume diffusion, while their activation energies should be much lower than the values listed here [34,35].

Intuitively, the diffusion process should not be solely controlled by the intrinsic thermally activated isolated V_{Zn}. In fact, the regular curve of the diffusion activation energy versus temperature can be divided into two parts: one of intrinsic control and one of extrinsic control [36]. Considering the finding that ΔH_a for D2 and D3 were obviously larger than that for D1, the present diffusion process can be reasonably attributed to the result of the Ga doping-induced extrinsic defects rather than the thermally activated intrinsic V_{Zn}. The defect chemistry was completely dominated by the extrinsic defects as the doping levels increased. Moreover, ΔH_a reached a minimum that corresponded to ΔH_m, the migration energy. Therefore, ΔH_a of D1 was almost identical to ΔH_m for the intrinsic V_{Zn}.

In this case, if the samples are doped further, ΔH_a will remain fixed, while D will increase because the concentration of the mobile defects will increase along with the increased Ga dopant atoms. As illustrated in Figure 2(b), the ^{68}Zn self-diffusion in D2 became more pronounced than in D1 at the same annealing temperature, indicating that larger quantities of extrinsic defects existed in D2 than in D1. Excluding the influence of the intrinsic V_{Zn} introduced by the thermal activation process, the enhanced self-diffusion behavior should only be caused by the dissociation of the V_{Zn}-related complex (more accurately, the $(Ga_{Zn}\text{-}V_{Zn})^-$ complex defect), which injected native defects during annealing [37]. The formation of the $(Ga_{Zn}\text{-}V_{Zn})^-$ complex defects was much easier in D3 because of its more O-rich growth condition, which was why the ^{68}Zn self-diffusion in D3 was also more enhanced than in D1 at 923 K (Figure 2(b)). Furthermore, the almost identical ^{68}Zn profile curves in Figure 1(a) served as a solid evidence for this argument. The negligible influence of the Zn/O-rich growth limit and the Fermi level on the ^{68}Zn concentration depth profiles of the as-grown samples indicated that the available isolated Zn vacancies had an ignorable effect on the diffusion of Zn atoms. Nevertheless, the

Downloaded to IP: 159.226.35.185 On: 2018-04-02 15:10:52 http://engine.scichina.com/doi/10.1007/s11433-018-9195-7

diffusion profiles at 923 K manifested a strong dependence on the Zn/O-rich growth condition and the Fermi level. This result suggested that the thermally dissociated Zn vacancies from the $(Ga_{Zn}\text{-}V_{Zn})^-$ complex dominated the diffusion process. In other words, the $(Ga_{Zn}\text{-}V_{Zn})^-$ complex defect, instead of the isolated V_{Zn}^{2-}, should be the prevailing acceptor in Ga-doped ZnO. ΔH_a of D1 was approximately equal to ΔH_m (an *in situ* pre-annealing was performed to the bottom ^{64}ZnO:Ga layer of D1 to dissociate the complex defects and eliminate their influence on the diffusion activation energy); hence, the energy difference (~0.78 eV) between D2 (or D3) and D1 should be the activation enthalpy for the dissociation of the $(Ga_{Zn}\text{-}V_{Zn})^-$ complex, also known as the binding energy. It is very close to the theoretical result (~0.75 eV) predicted by the density functional theory (DFT) calculations [11]. The binding energy of a complex is defined as the formation energy difference of a complex and its constituents. Theoretically, it is usually unaffected by E_F and μ variations, which is quite consistent with our experimental findings.

The electrical compensation effect of the $(Ga_{Zn}\text{-}V_{Zn})^-$ complex and its binding energy were further corroborated by the measurements of the temperature-dependent carrier concentrations of the S-series samples. Under a similar growth condition with D2, S1 was synthesized with a single Ga-doped ZnO epilayer structure (Table 1). The electrical activation energy of S1 was determined by fitting the carrier concentration curve with the following equation: $n \propto \exp(-E_a/k_B T)$ (Figure 4). The value (~(0.82±0.02) eV) well matched the binding energy of the $(Ga_{Zn}\text{-}V_{Zn})^-$ complex defect inferred from the zinc self-diffusion experiments (~0.78 eV), which further confirmed that the electrical compensation in Ga-doped ZnO should be induced by the dominant $(Ga_{Zn}\text{-}V_{Zn})^-$ complex acceptor defect [11].

Oppositely charged defects tended to form pairs and complexes, thereby changing the charge and the number of ionized donors. In Ga-doped ZnO, Ga_{Zn}^+ was easy to combine with zinc vacancy to form the defect complex, the singly charged $(Ga_{Zn}\text{-}V_{Zn})^-$, and the charge-neutral $(2Ga_{Zn}\text{-}V_{Zn})^0$ defect cluster. The formation of the three-defect complex, $(2Ga_{Zn}\text{-}V_{Zn})^0$, is statistically difficult because its formation requires the diffusion of Ga impurities. While the Ga diffusion was much slower than the Zn self-diffusion because of

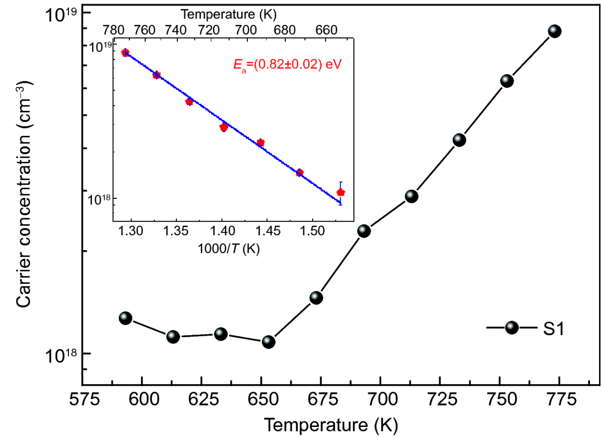

Figure 4 (Color online) Temperature dependence of the carrier concentration (n~T) over a temperature range of 593-773 K for S1. The Arrhenius plot for the temperature range of 653-773 K and the linear fitting are drawn in the inset.

the small impurity in the host-cation ratio [38], it is reasonable that the dissociation of the $(Ga_{Zn}\text{-}V_{Zn})^-$ complex, instead of $(2Ga_{Zn}\text{-}V_{Zn})^0$, is mainly involved in the annealing process. Therefore, after annealing at 1023 K, the carrier concentration of S1 increased from -9.88×10^{17} to -6.81×10^{19} cm^{-3}, suggesting that a large number of $(Ga_{Zn}\text{-}V_{Zn})^-$ were dissociated along with the diffusion of the Zn atoms and the annihilation of the zinc vacancies. Figure 5 demonstrates the detailed thermodynamic process. As a result, the electrical compensation effect caused by $(Ga_{Zn}\text{–}V_{Zn})^-$ was remarkably weakened, and the conductivity was recovered.

4 Conclusions

In conclusion, the investigation of the Zn self-diffusion behaviors in ZnO:Ga isotopic heterostructures with varied Zn/O-rich growth limit and Fermi level yielded the identification of the $(Ga_{Zn}\text{-}V_{Zn})^-$ acceptor complex defect as the predominant compensating center in Ga-doped ZnO. Its thermodynamic properties were successfully achieved by the combined SIMS and TDH measurements on the designed samples. The experimental binding energy of ~0.78 eV agreed well with the theoretical result. A self-consistent

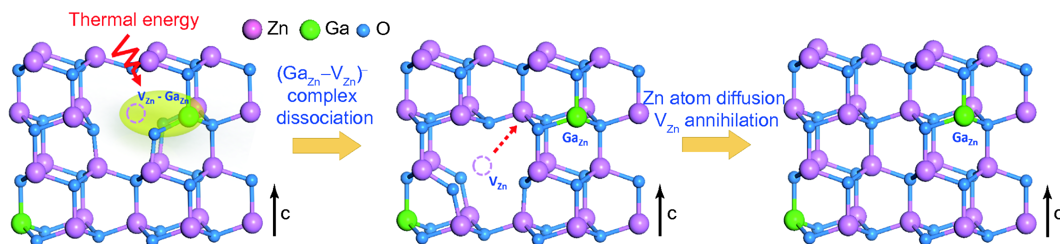

Figure 5 (Color online) Schematic thermodynamic process of the defect reactions in the annealing process, including the dissociation of the $(Ga_{Zn}\text{-}V_{Zn})^-$ complex, zinc atom diffusion, and annihilation of zinc vacancy.

Downloaded to IP: 159.226.35.185 On: 2018-04-02 15:10:52 http://engine.scichina.com/doi/10.1007/s11433-018-9195-7

electrical activation energy value of (0.82±0.02) eV was determined via the TDH measurements, further confirming the prevailing role of $(Ga_{Zn}\text{-}V_{Zn})^-$ in compensating for the carriers in Ga-doped ZnO. Overall, the results contribute to both the essential understanding and the potential engineering routes of the $(Ga_{Zn}\text{-}V_{Zn})^-$ complex defect in heavily Ga-doped ZnO.

This work was supported by the National Natural Science Foundation of China (Grants Nos. 11674405, and 11675280).

Supporting Information

The supporting information is available online at phys.scichina.com and http://link.springer.com/journal/11433. The supporting materials are published as submitted, without typesetting or editing. The responsibility for scientific accuracy and content remains entirely with the authors.

1 K. Ellmer, Nat. Photon. **6**, 809 (2012).
2 T. Minami, Semicond. Sci. Technol. **20**, S35 (2005).
3 P. D. C. King, and T. D. Veal, J. Phys.-Condens. Matter **23**, 334214 (2011).
4 P. R. West, S. Ishii, G. V. Naik, N. K. Emani, V. M. Shalaev, and A. Boltasseva, Laser Photon. Rev. **4**, 795 (2010).
5 D. C. Look, and K. D. Leedy, Appl. Phys. Lett. **102**, 182107 (2013).
6 S. Sadofev, S. Kalusniak, P. Schäfer, and F. Henneberger, Appl. Phys. Lett. **102**, 181905 (2013).
7 H. Kim, M. Osofsky, S. M. Prokes, O. J. Glembocki, and A. Piqué, Appl. Phys. Lett. **102**, 171103 (2013).
8 S. Kalusniak, S. Sadofev, and F. Henneberger, Phys. Rev. Lett. **112**, 137401 (2014).
9 T. Tyborski, S. Kalusniak, S. Sadofev, F. Henneberger, M. Woerner, and T. Elsaesser, Phys. Rev. Lett. **115**, 147401 (2015).
10 D. C. Look, K. D. Leedy, L. Vines, B. G. Svensson, A. Zubiaga, F. Tuomisto, D. R. Doutt, and L. J. Brillson, Phys. Rev. B **84**, 115202 (2011).
11 D. O. Demchenko, B. Earles, H. Y. Liu, V. Avrutin, N. Izyumskaya, Ü. Özgür, and H. Morkoç, Phys. Rev. B **84**, 075201 (2011).
12 J. T-Thienprasert, S. Rujirawat, W. Klysubun, J. N. Duenow, T. J. Coutts, S. B. Zhang, D. C. Look, and S. Limpijumnong, Phys. Rev. Lett. **110**, 055502 (2013).
13 J. Stehr, K. Johansen, T. Bjørheim, L. Vines, B. Svensson, W. Chen, and I. Buyanova, Phys. Rev. Appl. **2**, 021001 (2014).
14 A. Janotti, and C. G. van de Walle, Phys. Rev. B **76**, 165202 (2007).
15 P. Erhart, K. Albe, and A. Klein, Phys. Rev. B **73**, 205203 (2006).
16 R. Vidya, P. Ravindran, H. Fjellvåg, B. G. Svensson, E. Monakhov, M. Ganchenkova, and R. M. Nieminen, Phys. Rev. B **83**, 045206 (2011).
17 P. S. Xu, Y. M. Sun, C. S. Shi, F. Q. Xu, and H. B. Pan, Nucl. Instrum. Methods Phys. Res. Sect. B **199**, 286 (2003).
18 H. Zeng, G. Duan, Y. Li, S. Yang, X. Xu, and W. Cai, Adv. Funct. Mater. **20**, 561 (2010).
19 F. Tuomisto, K. Saarinen, D. C. Look, and G. C. Farlow, Phys. Rev. B **72**, 085206 (2005).
20 D. C. Look, J. W. Hemsky, and J. R. Sizelove, Phys. Rev. Lett. **82**, 2552 (1999).
21 S. J. Clark, J. Robertson, S. Lany, and A. Zunger, Phys. Rev. B **81**, 115311 (2010).
22 A. Azarov, V. Venkatachalapathy, Z. Mei, L. Liu, X. Du, A. Galeckas, E. Monakhov, B. G. Svensson, and A. Kuznetsov, Phys. Rev. B **94**, 195208 (2016).
23 L. Liu, Z. Mei, A. Tang, A. Azarov, A. Kuznetsov, Q. K. Xue, and X. Du, Phys. Rev. B **93**, 235305 (2016), arXiv: 1603.02831
24 L. Wang, L. Hsu, E. E. Haller, J. W. Erickson, A. Fischer, K. Eberl, and M. Cardona, Phys. Rev. Lett. **76**, 2342 (1996).
25 H. Bracht, E. E. Haller, and R. Clark-Phelps, Phys. Rev. Lett. **81**, 393 (1998).
26 H. Bracht, S. P. Nicols, W. Walukiewicz, J. P. Silveira, F. Briones, and E. E. Haller, Nature **408**, 69 (2000).
27 L. M. Wong, S. Y. Chiam, J. Q. Huang, S. J. Wang, J. S. Pan, and W. K. Chim, Appl. Phys. Lett. **98**, 022106 (2011).
28 B. Z. Dong, H. Hu, G. J. Fang, X. Z. Zhao, D. Y. Zheng, and Y. P. Sun, J. Appl. Phys. **103**, 073711 (2008).
29 P. Erhart, and K. Albe, Phys. Rev. B **73**, 115207 (2006).
30 J. Y. Noh, H. Kim, Y. S. Kim, and C. H. Park, J. Appl. Phys. **113**, 153703 (2013).
31 G. W. Tomlins, J. L. Routbort, and T. O. Mason, J. Appl. Phys. **87**, 117 (2000).
32 P. Erhart, and K. Albe, Appl. Phys. Lett. **88**, 201918 (2006).
33 H. Schmidt, M. Gupta, and M. Bruns, Phys. Rev. Lett. **96**, 055901 (2006).
34 M. A. N. Nogueira, W. B. Ferraz, and A. C. S. Sabioni, Mat. Res. **6**, 167 (2003).
35 J. C. Fisher, J. Appl. Phys. **22**, 74 (1951).
36 G. W. Tomlins, J. L. Routbort, and T. O. Mason, J. Am. Ceram. Soc. **81**, 869 (1998).
37 R. Kube, H. Bracht, E. Hüger, H. Schmidt, J. L. Hansen, A. N. Larsen, J. W. Ager, E. E. Haller, T. Geue, and J. Stahn, Phys. Rev. B **88**, 085206 (2013).
38 Y. Ke, S. Lany, J. J. Berry, J. D. Perkins, P. A. Parilla, A. Zakutayev, T. Ohno, R. O'Hayre, and D. S. Ginley, Adv. Funct. Mater. **24**, 2875 (2014).

Downloaded to IP: 159.226.35.185 On: 2018-04-02 15:10:52 http://engine.scichina.com/doi/10.1007/s11433-018-9195-7